

### 8.3 SPATIAL VARIABILITY AND GEOSTATISTICS

Soils vary continuously in space, especially when we consider domains at the soil series scale. However, our measurements of soil physical properties yield sets of discrete values for particular "point" locations within our soil sampling area. For a more complete interpretation of those discrete measurements, the theory of regionalized variables transforms our point discrete data to the soil continuum.

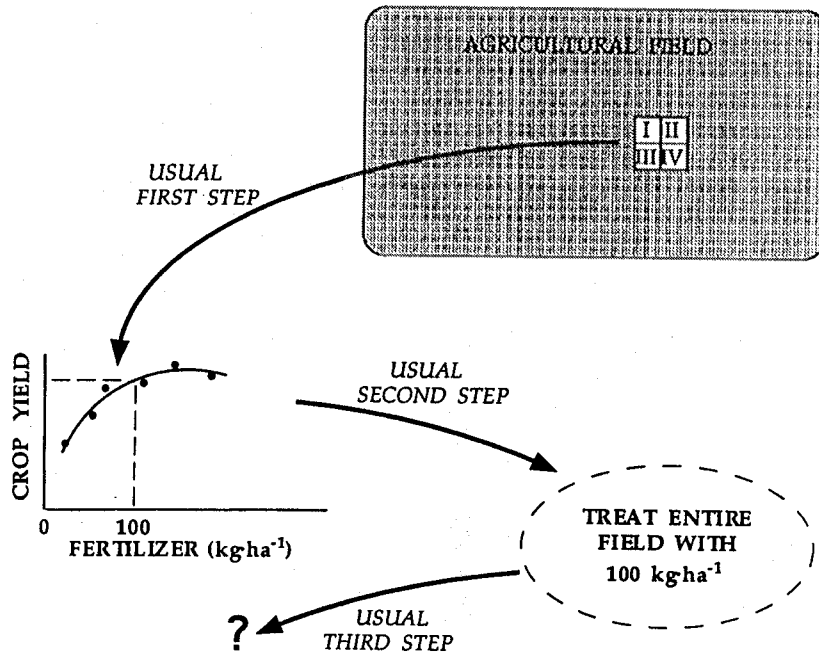


Figure 8.3. Small, replicated plot scheme typical of agricultural research.

Achievements in agricultural production have been aided by small, replicated plots established on sites believed to be "typical" or "representative" of a farmer's field or an agricultural landscape. Crop responses on these small plots treated with fertilizers, pesticides, irrigations, etc. were interpreted and formed the basis for uniformly treating an entire field. Figure 8.3 illustrates the all-too-common method today of conducting agronomic field research. In an agricultural field an experiment is located at a site which is assumed to be "representative" of the rest of the field as well as the soil of the agricultural region. With replicated treatments established in four statistical blocks, the first step is to establish the regression between crop yield and treatment. In this

example, a maximum yield is measured at about  $150 \text{ kg ha}^{-1}$  fertilizer. Being mindful of the desire not to waste fertilizer or pollute the subsoil environment with excess fertilizer and also noting that  $100 \text{ kg ha}^{-1}$  fertilizer produced a yield close to the maximum, the second step is a recommendation to apply  $100 \text{ kg ha}^{-1}$  fertilizer over the entire field. With an increased yield being obtained when the recommendation is followed, the farmer is happy. What is the usual third step taken in the above experimentation? It varies from repeating the same experiment or modifying its treatment levels, going to another field or soil condition or doing nothing more. Doing nothing more does not benefit the farmer nor does it benefit agriculture or the environment. Another sampling across the entire field could detect specific locations within the field where, for example, crop production could be increased, excessive levels of the fertilizer nutrient and deficiencies of other plant nutrients prevail or changes in soil quality indicative of achieving or denying sustainable agriculture are observed. Yes, another sampling across the entire field would ascertain if the farmer could make still further improvements in crop and soil management without necessarily imposing different treatments in still another replicated small plot experiment. Similar inefficient procedures can be found in research and in practical applications of soil hydrology.

Assuming steady-state conditions, deterministic concepts and mass balance equations have usually been applied for relatively short time periods – minutes, days, weeks or for times no longer than a growing season. Attempts to assess the impacts of agricultural methods and weather events between and during several growing seasons have been made through long-term experimental plots managed for decades, and in a few cases for more than a century. These kinds of experiments remain effective today when one wishes to ascertain the effect of a particular treatment relative to crop or animal production. On the other hand, they do little for improving our understanding of how agricultural practices impact on the quality of water leaving a cultivated field or rangeland. Moreover, they provide no direct information regarding the all-too-often subtle changes in soil quality occurring on a farm or within an agricultural region.

During the century, we have asked the question, "Does the treatment cause a significant perturbation from the expected mean?" We have used analysis of variance and regression techniques designed to minimize the impact of spatial or temporal heterogeneity in field soils and until recently, have not even taken the time to record where we take an observation within an experimental plot or field.

Regionalized variable analysis considers the distance between pairs of measured values as the main criterion in dealing with the variance. Here lies one of the main differences between classical "Fisher" statistics and geostatistics. Whereas the coordinate system is ignored in classical "Fisher" statistics, it is used in geostatistics to better answer the question, "How far apart should we take our samples?"

### 8.3.1 Autocorrelograms and Semivariograms

A geostatistical evaluation of data is performed using two tools; (i) the autocorrelogram and (ii) the semivariogram. Both tools can be used for data obtained in 1, 2 and 3 dimensions as well as in time. For the sake of simplicity here, we limit our description and their construction for sampling along a transect at regular intervals.

For an explanation of an autocorrelogram, we consider a transect of equidistant sampling and measurements of soil property *A*. We obtain a value of *A* at location  $x_1$  designated as  $A_1(x_1)$ , and similarly  $A_2(x_2), A_3(x_3) \dots A_n(x_n)$ , see Fig. 8.4. We compute correlation coefficients for pairs separated by a specified distance  $h$  using the relation

$$r(h) = \frac{\text{cov}[A(x), A(x+h)]}{\sqrt{\text{Var}[A(x)]}\sqrt{\text{Var}[A(x+h)]}} \quad (8.5)$$

For example, if we specify a distance  $h = 0$ , we find for pairs  $[A(x_i), A(x_i)]$  a correlation coefficient  $r_0 = 1$ . For pairs  $[A(x_i), A(x_{i+1})]$  at a distance  $h = 1$  (nearest neighbors), we obtain a value of  $r_1$ . Next, we increase the distance between the neighbors to  $h = 2$  for pairs  $[A(x_i), A(x_{i+2})]$  and obtain a value for  $r_2$  and so on. Details of the calculation are e.g. Webster, 1985; Webster and Oliver, 1990). Finally, we plot  $r_i$  versus  $h$  or  $r(h)$  and we obtain the function illustrated in Fig. 8.4. The distance between neighbors  $h$  is called the lag. The distance over which

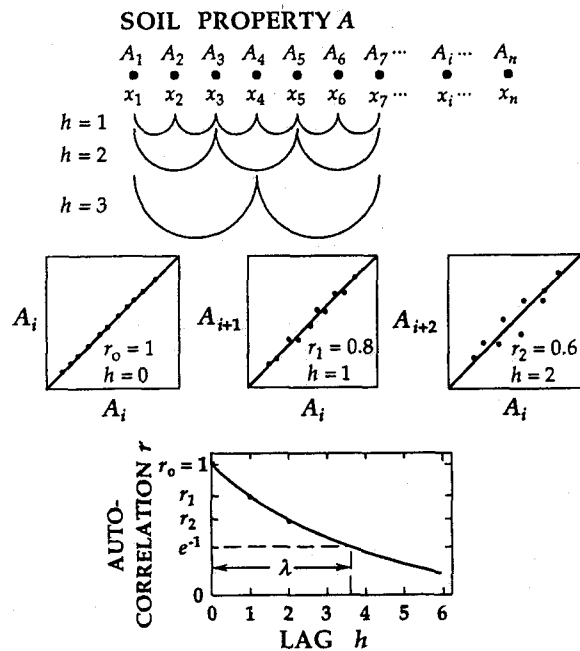


Figure 8.4. Derivation of the autocorrelogram with equidistant sampling along a transect.

a significant correlation exists is called the correlation length, scale, or range. Commonly, the correlation length  $\lambda$  is defined for a 1-dimensional transect by the relation

$$r = r_0 \exp(-x / \lambda) \quad (8.6)$$

where the value of  $r_0 = 1$  and that of  $r$  is diminished to  $e^{-1}$  at a distance of  $\lambda$ . Figure 8.5a presents soil water content  $\theta$  measured in a field at 1-m intervals with a neutron moisture meter at the 50-cm soil depth within a 160-m long transect. Neglecting the locations of the observations ( $n = 160$ ), the mean  $m$  and standard deviation  $s$  of the 160 observations are 0.136 and 0.0162  $\text{cm}^3 \cdot \text{cm}^{-3}$ , respectively. Figure 8.5b, the autocorrelogram of the 160 observations, shows that the autocorrelation length  $\lambda$  is about 6 m. Sampling at intervals less than 6 m is somewhat unnecessary because the observations are related to each other. Sampling at intervals greater than 6 m does not allow meaningful interpolation between neighboring observations. It should be obvious that the functional relation between  $r$  and  $h$  depends upon the size of the sample, and that in general, the greater the sample size, the greater the value of the autocorrelation length  $\lambda$ .

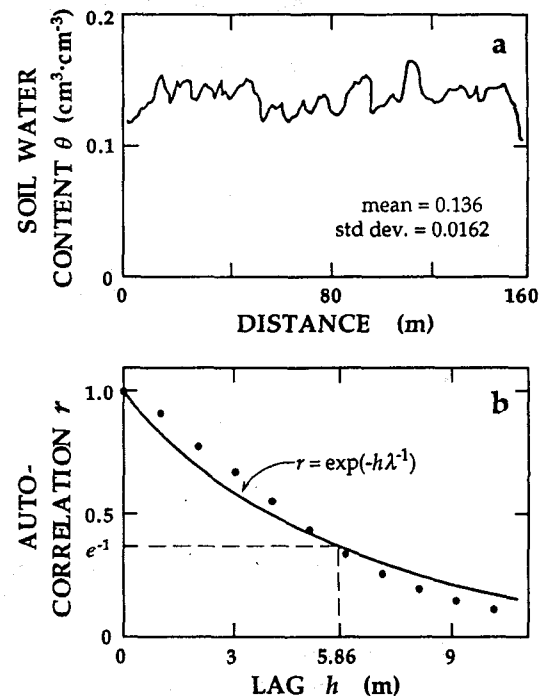


Figure 8.5. a. Values of soil water content  $\theta$  measured with a neutron probe along a 160-m transect at 1-m intervals. b. Autocorrelogram of  $\theta$  illustrating a correlation length  $\lambda$  of 5.86 m.

When we calibrate a soil moisture meter, we should try to sample at distances smaller than the value of  $\lambda$ . Or, when  $K_S$  is measured on samples of various sizes, autocorrelograms for each size provide estimates of  $\lambda$ . As the size of the sample increases, the value of  $\lambda$  or the scale of the autocorrelogram approaches an upper limit which defines the value of the REV. The same technique can be used to ascertain the magnitude of the REV of  $\theta$  for a particular value of  $h$ . Or by using different sampling volumes, we can establish equal autocorrelation scales for both  $\theta$  and solute content when we formulate transport equations for leaching.

The concept of autocorrelation is applicable only if second order stationarity exists, i.e. if the variance is constant across the field. Spatial trends across fields or within soil profiles can be found from autocorrelation functions. If there are shoulders within  $r(h)$  or if  $r(h)$  remains large as the separation distance increases, we can assume that trends exist. Because nonlinear trends yield different correlation scales for different sampling grid densities, trends along a transect can be examined by a regular dropping out of data to change the density of sampling. The correlation scale is also probably interrelated with transect spacing (Jury, 1989).

The concept of variance known from classical statistics is extended in geostatistics to consider the location of the observations  $[A(x_i), A(x_i + h)]$  separated by a distance  $h$ . The equation for the construction of the semivariogram is

$$\gamma(h) = \frac{1}{2n} \sum_{i=1}^n [A(x_i+h) - A(x_i)]^2 \quad (8.7)$$

As the distance between pairs of observations or lag  $h$  increases,  $\gamma(h)$  rises and asymptotically approaches the value of the variance called the sill, see Fig. 8.6. The sill is approached at  $h = \lambda$  denoted as the range or scale of the variogram as well as the zone of correlation. For  $h < \lambda$ , the variance is deformed by the position of the sampling points, or in other words, by the spatial dependence otherwise called the spatial structure. Methods for calculating  $\lambda$  are reviewed by Peck (1984). Semivariograms for spatially independent and dependent data as well as for a spatially changing domain are illustrated in Fig. 8.6. If the domain is spatially changing and not statistically homogeneous,  $\gamma(h)$  increases and does not approach a sill. Methods for dealing with this situation are described in the literature (e.g. Webster, 1985). The intercept at  $h = 0$  is called the nugget and usually appears as a consequence of fine scale estimates not being available. The nugget also includes the measurement error. Uehara et al. (1985) collected surface soil samples on a 1-km grid within a single soil series in Sudan extending over an area of about 400 km<sup>2</sup>. Additional samples only 1 m apart were also collected. Each sample was analyzed for exchangeable sodium percentage inasmuch as that soil attribute was judged to be most likely to limit sugarcane production. The spatial variance structure of the exchangeable sodium percentage across the domain is apparent in Fig. 8.7. The variogram has a nugget of 6.15, a range of 3 km and a sill and sample variance of 21.6. Kriged contours of exchangeable sodium percentage having values between 5 and 21% had a mean estimation variance of 10.5. (Kriging and co-kriging are discussed in the next section.)

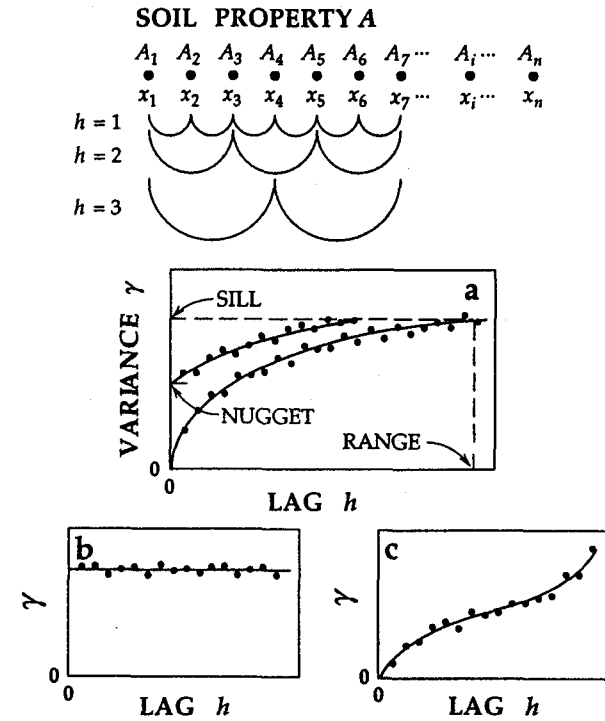


Figure 8.6. Derivation of the semivariogram with equidistant sampling along a transect: a. spatially dependent with and without a nugget, b. spatially independent and c. spatially changing domain.

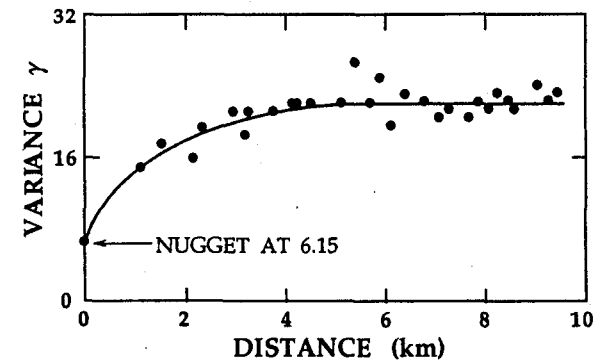


Figure 8.7. Semivariogram of exchangeable sodium percentage from samples taken on a 1-km grid over a 400-km<sup>2</sup> area of a mapping unit in Sudan (Uehara et al., 1985).

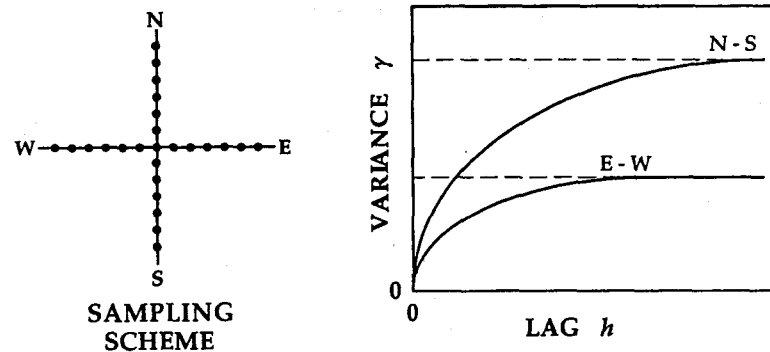


Figure 8.8. Semivariograms of two perpendicular transects of a non-isotropic domain.

In a non-isotropic domain variograms differ for different directions, see Fig. 8.8. For sampling on a rectangular grid, constructing variograms along the main two directions of the grid and on the two diagonals is a logical first choice to identify the presence of non-isotropic behavior. For the construction of the appropriate semivariograms, computed data  $\gamma(h)$  are fitted to a simple curve, usually the segment of a circle, or that of an exponential or hyperbolic curve. Interpreting semivariograms is made somewhat more reliable if a couple of "rules of thumbs" are followed. First, the minimum number of samples along a transect should be in the range of 50 to 100 (Gutjahr, 1985; and Webster, 1985). And second, the estimation of  $\gamma(h)$  is considered reliable for lags not exceeding 20% of the total transect length.

The term support refers to the size, shape and orientation of samples. An increase of support, called regularization, generally leads to a decrease of variation.

Reviewing data of various authors, Jury (1989) shows that the correlation length  $\lambda$  of a given soil property varies significantly. In some instances when the value of  $\lambda$  depends upon the sample spacing along the transect, we deal with a scale effect. In such cases, several theories provide an explanation (e.g. a violation of the stationarity hypothesis).

### 8.3.2 Kriging and Cokriging

Derived information on spatial variability in the form of  $r(h)$  and  $\gamma(h)$  can be advantageously used for estimating a soil property at locations where it is not measured. Kriging is a weighted interpolation named after D. G. Krige (1966) who devised it for estimating the gold content of ore in South Africa. Although its theoretical foundation was apparently recognized much earlier (Kolmogorov, 1941), its present day development is largely attributed to

Matheron (1965) and his associates. If  $A(x_1)$  and  $A(x_2)$  are measured values of  $A$  at locations  $x_1$  and  $x_2$ , respectively, we seek an unbiased estimate of  $A$  in between  $x_1$  and  $x_2$ . We interpolate with weights  $\mu$  and  $\nu$  for each of the positions  $x_1$  and  $x_2$ . Values of  $\mu$  and  $\nu$  depend upon the covariance function or the semivariogram as well as upon the location of the interpolated value. Note that the weights do not depend upon the actual values of  $A$ . The kriging variance or the minimum square error  $\sigma_K^2$  is a measure of the precision of the interpolated value. Many kriging formulations are available (e.g. Journel and Huijbregts, 1978). Here, we briefly introduce punctual kriging.

For  $n$  sampling points  $x_i$  ( $i = 1, 2, \dots, n$ ) in a field,  $A$  is estimated (or kriged) at  $x_0$  by

$$A^*(x_0) = \sum_{i=1}^n \lambda_i A(x_i) \quad (8.8)$$

where  $\lambda_i$  are the weights assigned to the sampling points and have a sum of unity. The kriging variance is

$$\sigma_K^2(x_0) = 2 \sum_{i=1}^n \lambda_i \bar{\gamma}(x_i, x_0) - \sum_{i=1}^n \sum_{j=1}^n \lambda_i \lambda_j \gamma(x_i, x_j) - \bar{\gamma}(x_0, x_0) \quad (8.9)$$

where  $\gamma(x_i, x_j)$  is the semivariance of  $A$  between the  $i$ th and  $j$ th sampling points,  $\bar{\gamma}(x_i, x_0)$  is the average semivariance between the  $i$ th sampling point and the field and  $\bar{\gamma}(x_0, x_0)$  is the average variance within the field. The kriging variance is least when

$$\sum_{i=1}^n \lambda_i \gamma(x_i, x_j) + \mu_L = \bar{\gamma}(x_j, x_0) \quad (8.10)$$

for all  $j$  where  $\mu_L$  is the Lagrange multiplier. The solution of (8.10) subject to the sum of the weights  $\lambda_i$  being unity provides values of the weights  $\lambda_i$  used in (8.8) as well as that of  $\mu_L$ . These values also allow estimation of  $\sigma_K^2(x_0)$  with

$$\sigma_K^2(x_0) = \sum_{i=1}^n \lambda_i \bar{\gamma}(x_i, x_0) - \bar{\gamma}(x_0, x_0) + \mu_L. \quad (8.11)$$

An example of kriging along a transect is given in Fig. 8.9. With kriging, additional optimal locations of sampling can be gained inasmuch as the kriged isolines depict more objectively the district of soils than an interpolation done by eye, or by linear interpolation between the measured data. The results of kriging depend upon the fitted semivariogram and can be easily validated as follows. An estimate of  $A$  is made for each location  $x_j$  for which an observation was obtained but is purposely left out of the kriging process. The procedure ("jack-knifing") is repeated for each of the measured  $j$  locations. The differences between the kriged and observed values are related to  $\sigma^2$ , and if equal to 1, the kriging procedure has been properly executed. The computational procedure is readily available in the literature (e.g. Journel and Huijbregts, 1978; and Webster, 1985).

In the derivation of the autocorrelogram we considered the spatial correlation of only one soil property with itself - hence, the term autocorrelation. The same principle can be applied to two properties  $A$  and  $B$  to determine to what extent property  $A$  at location  $x_i$  depends upon  $B$  at  $x_{i+1}$ . Here,



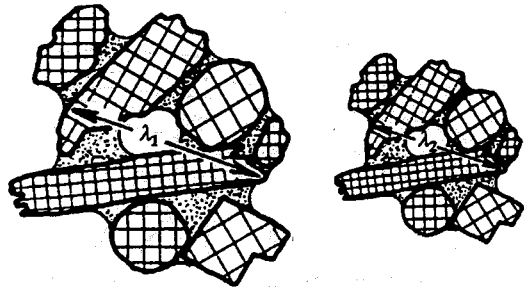


Figure 8.12. A self similar microscopic soil particle structure is the principle of Millers' scaling (Miller and Miller, 1956).

8.4 SCALING

Scaling theories are based upon the assumption that the continuously heterogeneous field is an ensemble of mutually similar homogeneous domains. We assume that each of the domains can be characterized by the SWRC  $h(\theta)$  which is related to the porous system through (4.11), or more generally by

$$h = f\left(\frac{1}{r}\right) \tag{8.12}$$

Two porous media of equal porosity are similar according to Miller and Miller (1956) when a scale factor  $\lambda$  exists which will transform one of the porous media to the other. Such similar media have identical microscopic structures except for scale, see Fig. 8.12. This kind of similarity leads to the constancy  $r_1/\lambda_1 = r_2/\lambda_2 = r_i/\lambda_i$  and to the formulation of a scaled, invariant pressure head  $h^*$  such that

$$\lambda_1 h_1 = \lambda_2 h_2 = \lambda_i h_i = \lambda^* h^* \tag{8.13}$$

where  $h^*$  can also be called an average pressure head and  $\lambda^*$  is an average scaling factor. Alternatively, we can denote the parameters of a reference soil with an asterisk.

Invariant microscopic flow in pores leads first to the formulation of an equation for the mean pore water velocity, see Hagen-Poiseuille (5.10) for laminar flow. Hence, the saturated hydraulic conductivity is

$$K_s = f(r^2) \tag{8.14}$$

and with the dimensionless term  $r/\lambda$ , we obtain

$$K_s^*/(\lambda^*)^2 = K_{si}/\lambda_i^2 \tag{8.15}$$

and analogously for  $K(\theta)$

$$K^*(\theta)/(\lambda^*)^2 = K_i(\theta)/\lambda_i^2 \tag{8.16}$$

where  $K_s^*$  and  $K^*(\theta)$  are either average values or values of a reference soil. The original scaling of Miller and Miller (1956) is restrictive in two aspects. First, a

microscopic length is physically interpreted, and second, the requirement of a constant porosity is rarely applicable.

Warrick et al. (1977) extended the use of the Millers' single scaling factor by introducing the degree of saturation (equivalent to the earlier relative soil water content  $\theta_R$ ) and eliminating the assumption of identical porosities. Thus, they scaled  $\theta$  with the scaling factor  $\theta_S$ . Additionally, their derivation of  $\lambda$  does not require a search for a microscopic physical length. For the derivation of  $\lambda$ , the sum of squares

$$\sum_{r,i} (h^* - \lambda_{r,i} h_i)^2$$

was minimized for  $r$  locations. Using this scaling procedure, a large dispersion of experimental data of  $h(\theta/\theta_S)$  and  $K(\theta/\theta_S)$  was nicely coalesced into unique functions, see Fig. 8.13. Hence, soil heterogeneity is approximated by the stochastic character of  $\lambda$  which retains its universal meaning with relations

$$\lambda = \frac{h^*}{h} \quad \lambda = \left(\frac{K}{K^*}\right)^{1/2} \quad \theta_R = \frac{\theta}{\theta_S} \tag{8.17}$$

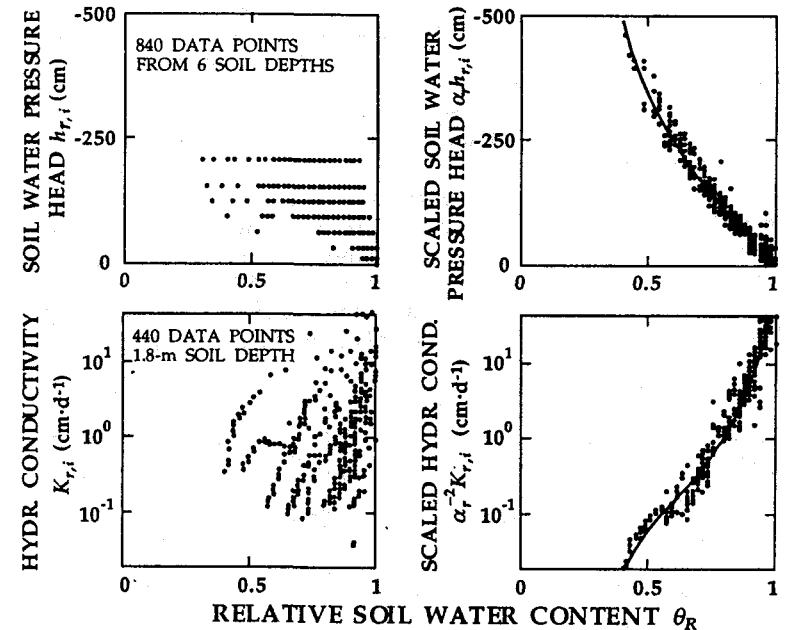


Figure 8.13. The scattering of experimental  $h_r(\theta_R)$  and  $K_r(\theta_R)$  data (left) is substantially reduced by Warrick's scaling (Warrick et al., 1977). The lines given in the upper and lower right hand graphs are the equations  $\{h = -6020 \theta_R^{-1} [(1 - \theta_R) - 2.14(1 - \theta_R)^2 + 2.04(1 - \theta_R)^3 - 0.694(1 - \theta_R)^4]\}$  and  $[\ln K = -20.5 + 75.0 \theta_R - 109 \theta_R^2 + 59.7 \theta_R^3]$ , respectively.

The modification for estimating  $\lambda$  indicated in the Warrick et al. (1977) procedure was fully developed by Simmons et al. (1979). They rejected the assumption of microscopic geometrical similarity and based their method on the similarity between soil hydraulic functions.

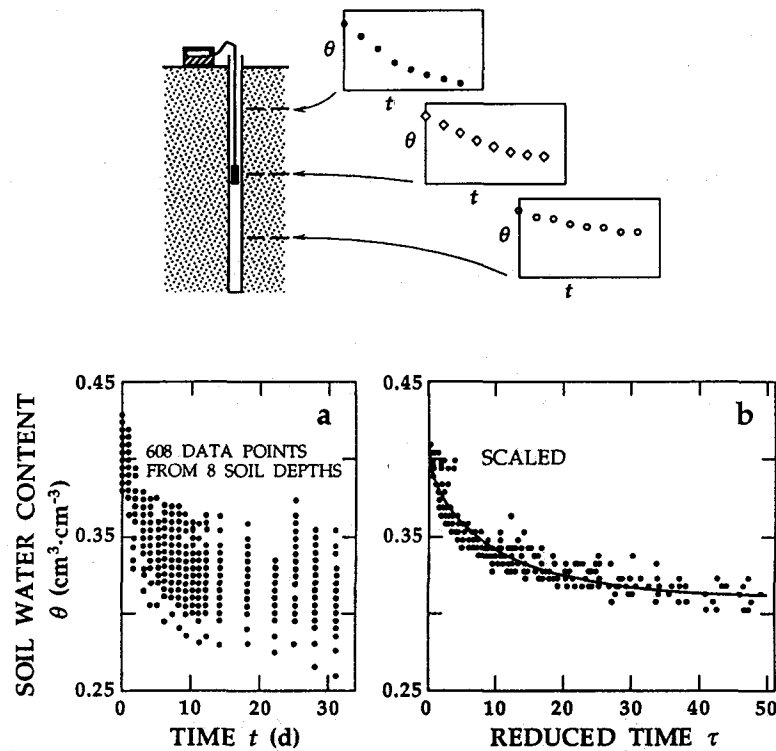


Figure 8.14. Neutron probe soil water contents measured at different soil depths and spatial locations during redistribution. Equation (8.18) is the solid line describing the scaled data.

Simmons et al. (1979) as well as others (see authors and those cited in Hillel and Elrick, 1990) have derived scaling relations that have not yet been sufficiently examined under field conditions to define criteria for their acceptance or rejection. Some of the formulations are physically based while others are mathematical techniques of inspectional analysis. Sposito and Jury (1990) showed that Richards' equation will be invariant under scaling transformations only if  $K(\theta)$  is a power or exponential function. If that is the case, the solution of Richards' equation obtained for one location can then be

scaled to other locations in the same field or domain. Assuming  $K(\theta)$  is an exponential function and a unit hydraulic gradient exists during redistribution in the absence of evapotranspiration, Simmons et al. (1979) recommended that (7.28) be scaled with a common value of  $\beta$  in (7.27) for all locations within a field. Fig. 8.14a shows soil water content versus redistribution time for a total of 608 measurements (19 times at 32 locations) within 4 plots covered by plastic sheeting to prevent evaporation after steady state infiltration had ceased. Fig. 8.14b shows the data from Fig. 8.14a, scaled with reduced time  $\tau$  and a common initial value of  $\bar{\theta}_0$ . The solid line in Fig. 8.14b is

$$\theta = \bar{\theta}_0 - \frac{1}{\beta} \ln \left[ 1 + \frac{\beta K^* \tau}{z^*} \right] \quad (8.18)$$

where  $\bar{\theta}_0 = 0.408 \text{ cm}^3 \cdot \text{cm}^{-3}$ ,  $\beta = 50$ ,  $K^* = 5.29 \text{ cm} \cdot \text{d}^{-1}$ ,  $z^* = 120 \text{ cm}$  and  $\tau = \omega^2 z^* (az)^{-1} t$  [ $a$  is defined in (7.26) and  $\omega$  is the scale factor for each location defined by  $K_0 = \omega^2 K^*$  where  $K$  is the scale mean of all  $K_0$ ]. The measured  $\theta$  deviate from the solid line with a pooled standard deviation is  $0.008 \text{ cm}^3 \cdot \text{cm}^{-3}$  – a value comparable to the neutron probe measurement error.

Methods based upon regression analysis are described as functional normalization techniques (Tillotson and Nielsen, 1984). With this approach being only macroscopic, geometrical similarity of the porous system is therefore not the condition for scaling. The idea of a universal  $\lambda$  for all hydraulic functions was abandoned as it was found that  $\lambda$  for scaling  $h(\theta_R)$  is not necessarily identical with that of  $K(\theta_R)$ . Even if the two scaling factors are different, they are generally correlated. In order to differentiate from the previous universal single set of scaling factors  $\lambda_i$ , we shall now use symbols  $\alpha_{1i}$  and  $\alpha_{2i}$  for the two sets of scaling factors, the first one denoting the scaling of  $h$  and the second denoting the scaling of  $K$ . Hence, we have

$$\alpha_1 = \frac{h^*}{h} \quad \alpha_2 = \left( \frac{K}{K^*} \right)^{1/2} \quad \theta_R = \frac{\theta}{\theta_s} \quad (8.19)$$

A set of sampling locations is similar if the soil hydraulic functions can be scaled. Warrick (1990) reviewed the application of this scaling in three different regions, while Clausnitzer et al. (1992) demonstrated that simultaneous scaling with  $\alpha_1$  and  $\alpha_2$  is not always as successful as independent scaling using a single scaling factor  $\lambda$  (our notation here).

Still yet another scaling proposal of Vogel et al. (1991) is based upon the assumption that the spatial variability of soil hydraulic functions has two components, one being linear and the other being non-linear. Supposing that the linear component is dominant, he proposed linear scaling with

$$\alpha_h = \frac{h}{h^*} \quad \alpha_K = \frac{K(h)}{K^*(h^*)} \quad \alpha_\theta = \frac{\theta(h) - \theta}{\theta^*(h^*) - \theta} \quad (8.20)$$

Any of the above types of scaling should be tested for the measured set of functions. For the selected type of scaling the invariant form of Richards' equation is applied together with the scaled boundary conditions. We can denote the soils as Warrick, or Simmons, or Vogel similar. Once successfully scaled, computed fluxes can be "descaled" for any given sampling point. Of

greater importance is the study of the variability of the scaling parameters by stochastic and geostatistical methods. Scaling yields higher quality data or more useful information when soil samples within one soil type are scaled independently from other soil types (Clausnitzer et al., 1992). The variability of soil hydraulic functions is appropriately expressed by scaling factors within each soil type where their pdf and correlation structure can be easily determined. Additional details on numerical procedures of scaling are described by Clausnitzer et al. (1992). Appropriate developments of dimensionless variables and scaled basic equations for various types of boundary conditions and soil hydrological problems have been assembled by Hillel and Elrick (1990).

Up to now we have demonstrated the scaling of soil hydraulic functions of field soils in order to ascertain reference soil parameters and the statistical character of the scaling factors. However, scaling techniques offer still a greater opportunity to formulate Richards' equation in an invariant form for the solution of elementary hydrological processes. Once a solution is known for a defined soil or boundary condition and is expressed in scaled variables, it is valid for all soils or boundary conditions within the given class of flow problem. Two different procedures are available. (i) Variables and soil hydraulic functions are scaled by the boundary condition with these scaled variables usually not being dimensionless. (ii) Variables are scaled to dimensionless forms using soil hydraulic functions. These solutions are similar to traditional expressions of solutions of flow problems in dimensionless variables.

The first procedure was used in the study of two scaling classes. (i) Infiltration with a constant flux at the soil surface (Neuman's boundary condition) and infiltration into a crust-topped soil (Kutilek et al., 1991). Variables  $z$ ,  $t$  and  $\theta$  scaled by the boundary condition, i.e. either using the flux density  $q_0$  (left-hand column) or using the resistance  $R$  (right-hand column) are

$$t = q_0^\alpha T^* \quad t = R^a T^* \quad (8.21)$$

$$z = q_0^\beta Z^* \quad z = R^b Z^* \quad (8.22)$$

$$\theta - \theta_r = q_0^\gamma \theta^* \quad \theta - \theta_r = R^c \theta^* \quad (8.23)$$

The soil hydraulic functions expressed in a power form  $D(\theta) = D_0(\theta - \theta_r)^n$ ,  $h(\theta) = -p(\theta - \theta_r)^m$  and  $K(\theta) = K_0(\theta - \theta_r)^p$  similarly scaled are

$$D(\theta) = q_0^{\alpha\gamma} D^*(\theta^*) \quad D(\theta) = R^{c\alpha} D^*(\theta^*) \quad (8.24)$$

$$h(\theta) = q_0^{\beta\gamma} h^*(\theta^*) \quad h(\theta) = R^{c\beta} h^*(\theta^*) \quad (8.25)$$

$$K(\theta) = q_0^{\gamma} K^*(\theta^*) \quad K(\theta) = R^{c\gamma} K^*(\theta^*) \quad (8.26)$$

And, Richards' equation in the diffusive form (5.68) transcribed into scaled variables invariant to  $q_0$  is

$$q_0^{(\gamma-\alpha)} \frac{\partial \theta^*}{\partial T^*} = q_0^{(\alpha\gamma+\gamma-2\beta)} \frac{\partial}{\partial Z^*} \left[ D^*(\theta^*) \frac{\partial \theta^*}{\partial Z^*} \right] - q_0^{(\gamma-\beta)} \frac{\partial K^*(\theta^*)}{\partial Z^*} \quad (8.27)$$

Similarly, (5.68) transcribed into scaled variables invariant to  $R$  is

$$R^{(c-\alpha)} \frac{\partial \theta^*}{\partial T^*} = R^{(c\alpha+\gamma-2\beta)} \frac{\partial}{\partial Z^*} \left[ D^*(\theta^*) \frac{\partial \theta^*}{\partial Z^*} \right] - R^{(c\gamma-\beta)} \frac{\partial K^*(\theta^*)}{\partial Z^*} \quad (8.28)$$

Boundary conditions are expressed in a similar manner. The exponents for the above conditions are

$$\alpha = \frac{-2m-n}{m+n+1} \quad a = \frac{2m+n}{2m+n+1} \quad (8.29)$$

$$\beta = \frac{-m}{m+n+1} \quad b = \frac{m}{2m+n+1} \quad (8.30)$$

$$\gamma = \frac{1}{m+n+1} \quad c = \frac{-1}{2m+n+1} \quad (8.31)$$

The solution of the infiltration problem plotted in scaled variables  $\theta^*(Z^*, T^*)$  is valid for the whole class, i.e. either for all variations of constant flux at the soil surface, see Fig. 8.15, or for all variations of resistance (except for  $R = 0$ ), see Fig. 6.25.

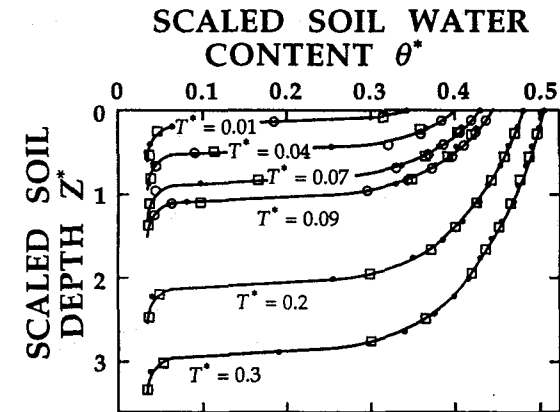


Figure 8.15. Scaling of Richards' equation through the boundary flux for NBC infiltration offers unique soil water profiles for all fluxes. Scaled variables are  $\theta^*$ ,  $Z^*$  and time  $T^*$  (Kutilek et al., 1991). The symbols  $\square$ ,  $\bullet$  and  $\circ$  designate values of  $q_0 = 0.05, 0.15$  and  $0.25 \text{ cm}\cdot\text{h}^{-1}$ , respectively. The value of  $K_S$  is  $0.196 \text{ cm}\cdot\text{h}^{-1}$ .

The second scaling procedure elaborated by Warrick and Hussen (1993) is applicable to a broader family of flow classes, e.g. redistribution and upward flow. They defined the dimensionless variables

$$Z^* = z/z_0 \quad T^* = t/t_0 \quad (8.32)$$

and functions

$$\theta^* = \frac{\theta - \theta_r}{\theta_0 - \theta_r}, \quad K^* = K/K_0, \quad h^* = h/z_0 \quad (8.33)$$

where  $\theta_0 \leq \theta_s$  and  $K_0 = K(\theta_0)$ . When they considered the soil hydraulic characteristics

$$\frac{\theta - \theta_r}{\theta_s - \theta_r} = \left( \frac{h_A}{h} \right)^\lambda \quad \frac{K}{K_r} = \left( \frac{\theta - \theta_r}{\theta_s - \theta_r} \right)^n \quad (8.34)$$

they defined

$$z_o = |h_A| \left( \frac{\theta_o - \theta_r}{\theta_s - \theta_r} \right)^{-1/\lambda} \quad (8.35)$$

and

$$t_o = \frac{(\theta_o - \theta_r) z_o}{K_o} \quad (8.36)$$

Hence, in Richards' equation all variables and soil hydraulic functions are scaled with each equation being invariant and dimensionless. An example of a scaled soil water profile  $\theta^*(Z^*, T^*)$  for infiltration with DBC is given in Fig. 8.16.

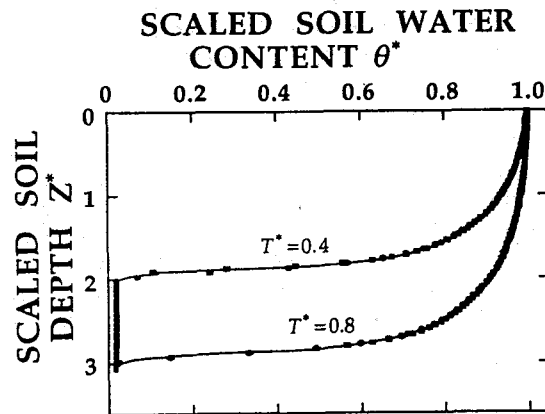


Figure 8.16. Soil water profile for Guelph loam (Warrick and Hussen, 1993) in scaled variables  $\theta^*(Z^*, T^*)$  for DBC infiltration is unique in  $\theta^*(Z^*)$  for  $T^* = 0.4$  and  $0.8$ . Data points represent the following combinations of saturated hydraulic conductivity ( $\text{cm}\cdot\text{h}^{-1}$ ) and relative soil water content [ $K_s, \theta_o/\theta_s$ ]: [1.332, 1.0], [2.664, 1.0], [1.332, 0.9] and [2.664, 0.9].

A scaling procedure is also advantageous for the solution of the inverse problem of infiltration (Warrick, 1993). With the soil hydraulic functions being scaled together with variables, the procedure is conveniently reduced to simple algebraic computations instead of repetitive numerical simulations.

## 8.5 STATE-SPACE EQUATIONS FOR MULTIPLE LOCATIONS

A state-space solution was introduced (section 7.3.2.2) in order to ascertain  $K(\theta)$  within prescribed fiducial limits for a pedon. That state-space formulation described soil water redistribution with an approximate ordinary first-order differential equation, assumed  $K(\theta)$  to be of exponential form and quantitatively included the uncertainty of the neutron probe and its calibration. Here we present a similar analysis to compute evaporation between irrigation events as well as to determine a soil water diffusivity function from soil water profiles measured at multiple locations within a field. The uncertainties associated with soil heterogeneity as well as those of instrument calibration are separately identified.

Five neutron access tubes positioned every 18 m along a transect allowed soil water content to be monitored with a neutron probe at 15-cm depth intervals within the soil profile at each location. The level site was free of vegetation and equipped with a sprinkler irrigation system that was used to apply 15 small irrigations (each <20 mm) during a 3-month period. In addition to the neutron probe measurements of soil water to estimate evaporation, 20-min weighings of a 50-t capacity lysimeter in the same field were integrated to obtain daily values of evaporation.

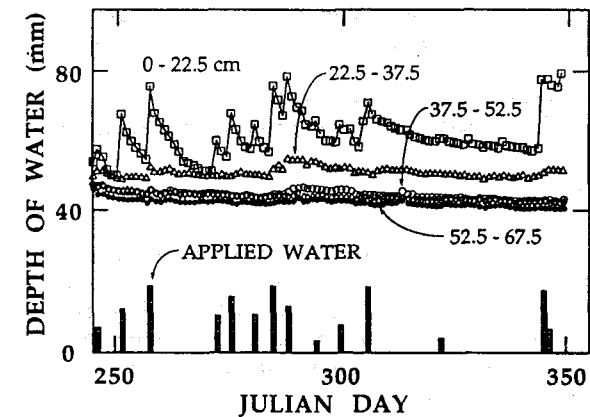


Figure 8.17. Depths of water stored within five depth intervals of a pedon measured with a neutron probe together with depths of water applied to the soil surface during the experiment. The depth interval 67.5 - 82.5 cm is represented with  $\diamond$  symbols.

The spatially averaged amounts of water stored within the five depth intervals of the soil profile measured with the neutron probe as a function of time together with the amounts of water applied with the sprinklers are shown in Fig. 8.17. Notice that the water stored in the lower depth intervals does not

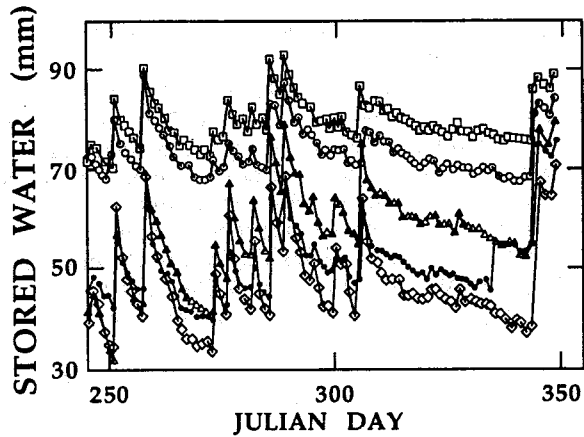


Figure 8.18. Depths of water stored within the 0 - 22.5 cm topsoil at each of five field locations measured with a neutron probe.

appreciably change during the entire experiment. Evaporation and infiltration from the applied water are the primary physical processes that create changes in stored water and those changes occur primarily in the 0 - 22.5 cm depth. Variations in soil water stored in the top 22.5 cm of the profile as a function of time as well as location are shown in Fig. 8.18.

The hydrologic balance in the absence of lateral flow and negligible drainage is

$$\frac{dS}{dt} = P_t - E_t \quad (8.37)$$

where  $S$  is the depth of stored water between the soil surface ( $z = 0$ ) and some depth  $b$  ( $b$  is the depth assumed to be uniformly wet),  $E_t$  the evaporation rate and  $P_t$  the rate at which water is applied to the soil surface (precipitation or irrigation). The evaporation rate can be calculated using the diffusion equation (assuming isothermal and homogeneous soil conditions)

$$\frac{\partial \theta}{\partial t} = \frac{\partial}{\partial z} \left[ D(\theta) \frac{\partial \theta}{\partial z} \right] \quad (8.38)$$

where  $D(\theta)$  is the soil water diffusivity function. Gardner (1962) obtained the following approximate solution of the depth-integrated form of (8.38)

$$E_t = \frac{\pi^2 S D(S/b)}{4b^2} \quad \frac{Dt}{b^2} > 0.3 \quad (8.39)$$

where the diffusivity is a function of stored water  $S$ . Combining (8.37) and (8.39) the hydrologic balance becomes the ordinary differential equation

$$\frac{dS}{dt} = P_t - \left( \frac{\pi}{2b} \right)^2 S D(S). \quad (8.40)$$

For an exponential diffusivity function  $D(S/b) = A \exp(BS/b)$ , the state-space

equation for (8.40) is

$$dX_t = \left[ P_t - \left( \frac{\pi}{2b} \right)^2 X_t A \exp(BX_t/b) \right] dt + v_s dt \quad (8.41)$$

where  $X_t$  is the state variable representing the stored water  $S$  and  $v_s dt$  is a stochastic noise owing to the uncertainties in the proposed equation. The noise  $v_s dt$  arises owing to the various simplifying assumptions of the physical model such as neglecting thermal and salinity effects, swelling and shrinkage, hysteresis, etc. The corresponding observation equation at time  $t_k$  ( $k = 1, 2, 3, \dots$ ) is

$$Z_m(t_k) = X_t + v_m(t_k) \quad (8.42)$$

where  $Z_m$  is the observed amount of stored water at time  $t_k$  and  $v_m$  is the observation noise.

The diffusivity parameters  $A$  and  $B$  were calculated assuming that the observation variance  $R_t$  can be estimated from spatially averaging the neutron probe readings from the five access tubes located 18 m apart. It can be seen in Fig. 8.19 that the observation variance  $R_t$  is much larger than the neutron probe calibration variance. Values of  $A$  and  $B$  were estimated to be  $0.0292 \text{ mm}^2 \cdot \text{d}^{-1}$  and  $32.59$ , respectively, with the state variance per unit time  $Q$  being  $18.87 \text{ mm}^2 \cdot \text{d}^{-1}$ . The value of  $Q$  is of the same order of magnitude as the neutron probe calibration variance, while the model uncertainty for stored water prediction on a daily basis is within the neutron probe noise. The agreement found between the state space estimation of cumulative evaporation and that measured with the lysimeter ( $r^2 = 0.98$ ) indicates that the estimated diffusivity function provides an adequate description of evaporation and the soil water transport process.

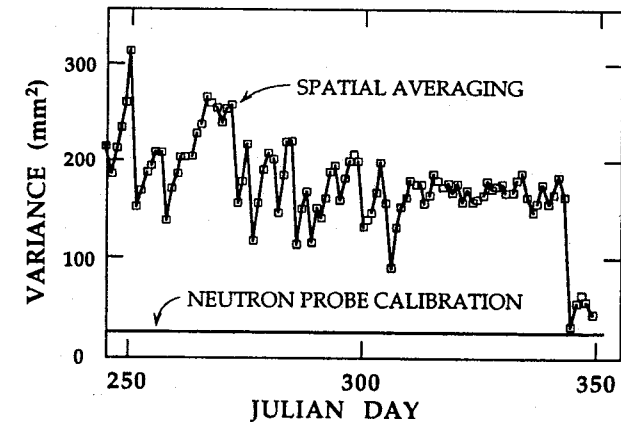


Figure 8.19. Observation variance owing to spatial averaging of measured soil water storage for the 0 - 22.5 cm topsoil as well as the variance of the neutron probe calibration.

State-space formulations that describe location-averaged phenomena could improve our understanding of the development of soil horizons, growth and water extraction of plant roots and chemical and microbiologically-induced reactions within soil water. We also expect that progress could be made using time-averaged equations to examine critical periods during which soil processes occur; these soil processes may be related to particular soil locations, mapping units or regions.

## PROBLEMS

1. Derive the scaled cumulative infiltration term  $I^*$  for infiltration into the crust-topped profile. Use scaled variables and functions of Kutilek et al. (1991).
2. Values of soil property  $A(x)$  have been measured along a transect at three locations:  $A(1) = 7$ ,  $A(2) = 5$  and  $A(4) = 3$ . a. Using a simple desk calculator, estimate  $A(3)$  by kriging. Hint: After calculating the only value possible of  $\gamma(h)$  with (8.7) for each of the lags (1, 2 and 3), estimate a smooth variogram  $\gamma(h) = mh^b$  by regression. Using values of  $\gamma(h)$  from the regression at  $h = 1, 2$  and  $3$ , calculate the weights  $\lambda_i$  with (8.10). b. What is the value of the kriging variance for  $A(3)$ ?
3. You have measured infiltration with double ring infiltrometers every 5 m along a 500-m transect. Two different inner ring diameters were used. The diameter  $d$  was a. 50.5 cm and b. 25.2 cm. The diameter of the outer ring  $D = 2d$ . The evaluated semivariograms are in Fig. 8.6a with nugget for  $d = 50.5$  cm and in Fig. 8.6b for  $d = 25.2$  cm. What are your conclusions regarding an appropriate size of the ring and the range of the variograms?
4. You are calibrating a neutron probe. Recognizing that the autocorrelogram in Fig. 8.5 had been previously determined in your field, sketch the locations of 4 soil sampling sites for measuring the soil water content around the access tube.
5. Estimate the range of the variograms for sand,  $pF = 2.5$ , silt and AWC in Fig. 8.10. Would you expect the range of a variogram of quasi-steady state infiltration rate to be more or less than 25m?
6. How will you scale infiltration rate and cumulative evaporation if the scaling factors are expressed by (8.19)?
7. Show the relation between (8.39) and (7.3).
8. a. Starting with (7.25) and (7.27) and assuming  $a = 1$  and  $b = 0$  in (7.26), derive the following expression for the flux density at soil depth  $L$ :

$$q_L = K_o \left( 1 + \beta K_o t L^{-1} \right)^{-1}$$

- b. Assuming the mean values of  $K_o$  and  $\beta$  are  $31.9 \text{ cm}\cdot\text{d}^{-1}$  and  $61.1$ , respectively, calculate  $q_L$  at a soil depth of 1.8 m for  $t = 1$  and 10 d.
9. The probability distribution function of  $K_o$  in problem 7 is divided into five 20%-fractile groups having median values of  $K_o = 1.98, 5.73, 11.9, 24.9$  and

$72.0 \text{ cm}\cdot\text{d}^{-1}$ . Similarly, the five 20%-fractile groups of  $\beta$  have median values of  $\beta = 22.1, 35.8, 49.9, 69.6$  and  $112.8$ . Assuming that the two probability distribution functions are independent, substitute into the equation of problem 7 each of the five median values of  $K_o$  with each of the five median values of  $\beta$ . to obtain 25 estimates of  $q_L$  (each of 4% probability) for  $t = 1$  d. From the 25 values, calculate the mean value  $\bar{q}_L$ . Repeat the calculations for  $t = 10$  d. Considering the 25 estimates of  $q_L$  and the mean  $\bar{q}_L$  and comparing these values with those of problem 7, discuss the implications for sampling a field to estimate  $\bar{q}_L$ .